

# Large Field-of-View Spectropolarimetric Observations with a Large Aperture Telescope

G. Molodij · G. Aulanier

Received: 15 October 2010 / Accepted: 15 October 2011 / Published online: 25 November 2011  
© Springer Science+Business Media B.V. 2011

**Abstract** In the context of the increasing interest in large-aperture telescopes dedicated to the Sun, we present a study to evaluate the adaptive-optics system limitations on the requirements expected for magnetic-field extrapolations and data-driven MHD simulations of active regions. The questions we address include: What is the size of the field of view at high spatial resolution for a four-meter class telescope with a spectrograph? What is the impact of the selected spectral domain on the performance in relation to the aforementioned scientific goals? We show that the visible-wavelength domain remains difficult to explore with ground-based telescopes using classical adaptive optics systems. The field of view obtained will be only a few arcseconds at the diffraction limit for most of the time. We review alternative configurations of adaptive-optics systems for different telescope apertures and wavelength domains which could be considered for practical implementation in derivations of the magnetic field from polarimetric observations.

## 1. Introduction

Solar physics research requires observations of magnetic features in a challenging range, from one-tenth of an arcsecond for flux tubes, to a few arcminutes for active regions. Another demand on the image-compensation system is that the observer should be able to analyze a broad field of view, in order to extrapolate the magnetic field. Focused studies of small  $\delta$ -spots only require relatively small fields of view, about 1.6 arcminutes; see Canou *et al.* (2009). However, the typical field of view required for extrapolation purposes is larger than two arcminutes: typically three to four arcminutes for emerging active regions, sigmoids, and medium-sized filaments (Aulanier and Schmieder, 2002; Pariat *et al.*, 2004; Schrijver *et al.*, 2008; Canou and Amari, 2010), and up to six arcminutes for large filaments, full AR studies, and later use of the results and initial conditions for MHD simulations (Lionello *et al.*, 2002; Metcalf *et al.*, 2008; Masson *et al.*, 2009). Adaptive optics (AO) is used to

---

G. Molodij (✉) · G. Aulanier  
LESIA-Observatoire de Paris-Meudon, CNRS, Université Pierre et Marie Curie-Paris 06,  
Université Paris Diderot-Paris 07, 5 place J. Janssen, 92190 Meudon, France  
e-mail: [guillaume.molodij@obspm.fr](mailto:guillaume.molodij@obspm.fr)

recover diffraction-limited resolution with large ground-based telescopes by compensating, in real time, atmospheric turbulence. However, adaptive optics requires a reference source close to the object of interest in order to accurately sense the wavefront disturbed by turbulence. The efficiency of the compensation by adaptive optics is limited by the conventional anisoplanatism effect (Fried, 1962). The wavefronts incoming from two structures on the Sun are different because of their different paths through the atmosphere. This effect limits the field of view around the reference source where a useful correction can be achieved.

High image quality is important for the observation of small solar magnetic features such as magnetic flux tubes. Nevertheless, accurate magnetic field topology studies, which involve relatively small flux concentrations, require not only good spatial resolution but also a homogeneous compensation of the terrestrial turbulence effects over an extended field of view. In order to evaluate the limitations due to anisoplanatism, we present tools to determine the quality of the measurement of the magnetic field after adaptive-optics compensation.

We analyze the nonlinear degradation of the measurements of the magnetic field performed with a long-slit spectrograph system and polarimetric data performed on large fields of view, taking into account the effects of anisoplanatism of turbulence of the terrestrial atmosphere. We analyze the spectra obtained from high spatial-observations performed with a ground-based long-slit spectrograph to determine the specific requirements of spectropolarimetry. The magnetic maps are the result of a scan made of successive steps with the spectrograph slit. The spatial resolution is determined by the spectrograph-slit width, but the filling factor of the magnetic flux depends on the image quality. High image quality for the observation of small solar magnetic features is necessary so that the light passing through the spectrograph entrance slit will come from the same solar structure throughout the integration time. Moreover, a precise image stabilization along the entire scan is an important requirement to compensate for motions coming from instrument vibrations and tracking errors (Molodij *et al.*, 1998).

In Section 2, we derive new simple analytic laws to evaluate both the size of the corrected field of view and the image quality for any classical AO system and telescope aperture. We review the problem of magnetic-field measurement at high spatial resolution with a long-slit spectrograph in Section 3. We simulate the effect of anisoplanatism for an implementation of a low-order AO system in the infrared wavelength range, and we discuss the implications of the results on high spatial resolution projects envisioned in the future, in the context of full active-region observations as input for coronal models.

## 2. Theoretical Background

In this section, we present simple analytic laws to evaluate both the size of the corrected field of view and the image quality for any classical AO system and telescope aperture. Theoretical techniques to evaluate the effects of anisoplanatism on the performance of an AO system are detailed in Appendix A. We show in the following subsections that the behavior of the isoplanatic field of view after AO correction [ $\theta_{\text{cor}}$ ] and the image quality after AO correction [ $\sigma_J^2$ ] are expressed as

$$\begin{aligned}\sigma_J^2 &\propto \left(\frac{D^2}{J}\right)^{\frac{5}{6}}, \\ \theta_{\text{cor}} &\propto \frac{D}{\sqrt{J}},\end{aligned}\tag{1}$$

where  $J$  is the number of compensated modes and  $D$  the telescope aperture.

These two functions are useful tools for evaluating the AO system limitations with regard to the scientific requirements expected for magnetic-field extrapolations and data-driven MHD simulations of active regions.

### 2.1. Determination of the Isoplanatic Field of View after AO Compensation

Considering an AO system of  $J$  degrees of freedom, the object wavefront  $[\phi_{\text{obs}}]$  is corrected by the phase reconstruction at the  $J$ th order of the reference wavefront  $[\phi_{\text{ref}}]$  separated by an angle  $\alpha$ . The residual phase variance after correction is (using the notation of Appendix A)

$$\sigma^2(\alpha) = \sum_{j=J+1}^{\infty} \langle (a_j)^2 \rangle + 2 \sum_{j=2}^J [\langle (a_j)^2 \rangle - \langle a_j^{(\text{obs})} a_j^{(\text{ref})} \rangle(\alpha)], \tag{2}$$

where the first term of the equality is the residual variance due to the limited number of modes (Noll residual) and the second term corresponds to the anisoplanatism error after  $J$  compensated modes.

The residual variance optimization in terms of field of view, *i.e.* for a given angle, is obtained when for each polynomial  $j$  satisfies

$$\langle (a_j)^2 \rangle - \langle a_j^{(\text{obs})} a_j^{(\text{ref})} \rangle(\alpha) > 0. \tag{3}$$

This is the case when the normalized correlation function of the  $j$ th mode is larger than 50%. The residual variance is then reduced. The analytic expression of the 50% correlation function  $[C_{1/2}]$ , introducing the polynomial radial degree  $n$  related to the polynomial  $j$  by the relation  $2j = (n + 1)(n + 2)$ , the Bessel function of the  $n$ th order  $J_n$ , the spatial frequency  $K$ , and the telescope diameter pupil  $D = 2R$ , is (see details in Appendix A)

$$C_{1/2}(\alpha, n, D) = \frac{1}{2} = \frac{\int_0^\infty dh C_n^2(h) \int_0^\infty dK K^{-14/3} J_{n+1}^2(K) J_0(\frac{\alpha h K}{R})}{\int_0^\infty dh C_n^2(h) \int_0^\infty dK K^{-14/3} J_{n+1}^2(K)}. \tag{4}$$

The measured wavefront at angular distance  $\alpha$  provides a satisfactory fit of the on-axis wavefront when the correlation criterion of Equation (4) is satisfied for all of the correction modes (Molodij, 2011).

Figure 1 shows the normalized angular correlation of the Zernike coefficients allowed for an angular separation  $\alpha$  normalized by the telescope radius  $R$ . This criterion allows us to select the number of useful correction modes for a given angular distance between the two wavefronts. Keeping in mind that all of the low orders must first be corrected, a higher-order mode will be corrected only if the criterion is verified. This result is general in wavefront-residual variance estimation in AO using modal analysis (Rousset, 1993).

In the following, we derive the optimal modal compensation behavior with respect to the field of view, assuming that Equation (4) is an absolutely convergent integral and that the different modes are related to the turbulence-profile distribution only with respect to the power spectra; *i.e.*  $C_n^2(h)$  is a constant (see Appendix C). The numerator of Equation (4) can be expressed as

$$\text{Constant} \times \int_0^\infty dK K^{-14/3} J_{n+1}^2(K) \int_0^\infty dh J_0\left(\frac{\alpha h K}{R}\right). \tag{5}$$

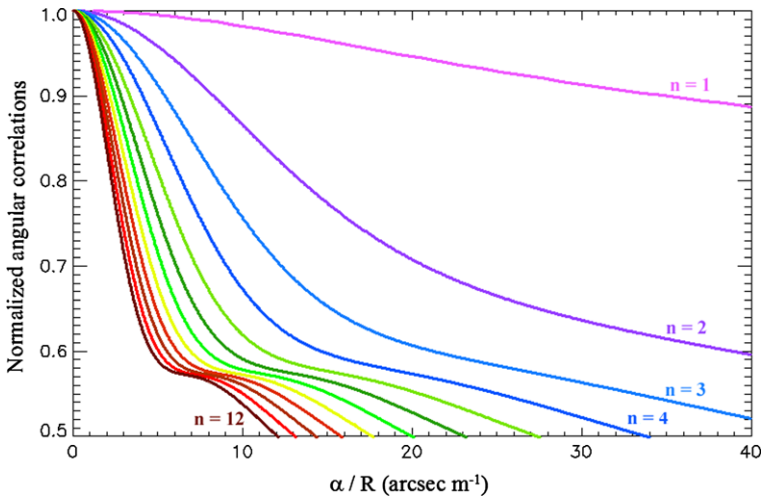


**Figure 1** Angular correlation per radial degree  $[n]$  of the Zernike coefficients *versus* the angular separation  $[\alpha]$ , between the object and the reference target, normalized by the telescope radius  $[R]$ . Curves are for different radial degrees  $n = 1$  to 12, calculated with the Hufnagel profile. Low-order polynomials are much more correlated than the higher orders.

The integral of  $h$  can be expressed by a Mellin transform,

$$F_m(s) = \int_0^\infty x^{s-1} f(x) dx, \tag{6}$$

with  $s = 1$  and using the transform properties  $f(ax) \rightarrow a^{-s} F_m(s)$ . One obtains

$$\int_0^\infty dh J_0\left(\frac{\alpha h K}{R}\right) = \left(\frac{\alpha K}{R}\right)^{-1}. \tag{7}$$

The 50% correlation function can be rewritten as

$$\int_0^\infty dK K^{-14/3} J_{n+1}^2(K) \left[1 - \frac{D}{\alpha K}\right] = 0. \tag{8}$$

Two expressions of the Bessel functions  $J_{n+1}$  can be derived from the asymptotic development at high and low frequency,

$$\begin{aligned} \text{Low frequency: } J_\nu(K) &\rightarrow \frac{1}{\nu!} \frac{1}{2^\nu} K^\nu, \\ \text{High frequency: } J_\nu(K) &\rightarrow \sqrt{\frac{2}{\pi K}} \cos\left(K - (2\nu + 1)\frac{\pi}{4}\right), \end{aligned} \tag{9}$$

with  $\cos^2(K - (2\nu + 1)\frac{\pi}{4}) \approx \frac{1}{2}$  if  $K \rightarrow \infty$ .

A cutoff frequency can be defined at the curve intersections at low and high frequency for each radial degree:

$$\left[\frac{1}{(n+1)!} \frac{1}{2^{n+1}} K_c^{n+1}\right]^2 = \frac{1}{2\pi K_c}, \tag{10}$$

with Stirling’s approximation for large  $n$ :

$$(n + 1)! \approx (n + 1)^{n+1} \exp(-(n + 1))\sqrt{2\pi(n + 1)}. \tag{11}$$

One derives that the cutoff frequency is proportional to  $n + 1$  to conclude that the Zernike polynomial of order  $n$  can be evaluated by Fourier modes corresponding to spatial frequencies  $K(n)$  (Conan and Madec, 1994). The analogy between Zernike polynomials and Fourier modes allows us to simplify the 50% correlation functions as

$$\int_0^\infty dK K^{-14/3} \delta(K - K(n)) \left[ 1 - \frac{D}{\theta_{\text{cor}} K} \right] = 0, \tag{12}$$

$$\theta_{\text{cor}} = \frac{D}{K(n)} \approx \frac{D}{n + 1},$$

where  $\delta$  is the Dirac function.

The behavior of the correlation function of the last corrected Zernike polynomial [ $N_{\text{max}}$ ] can be written as

$$\theta_{\text{cor}} \propto \frac{D}{N_{\text{max}}} \quad \text{or} \quad \theta_{\text{cor}} \propto \frac{D}{\sqrt{J}}, \tag{13}$$

with  $N_{\text{max}} \geq 2$  and the number of polynomials,  $J = \frac{(n+1)(n+2)}{2}$ .

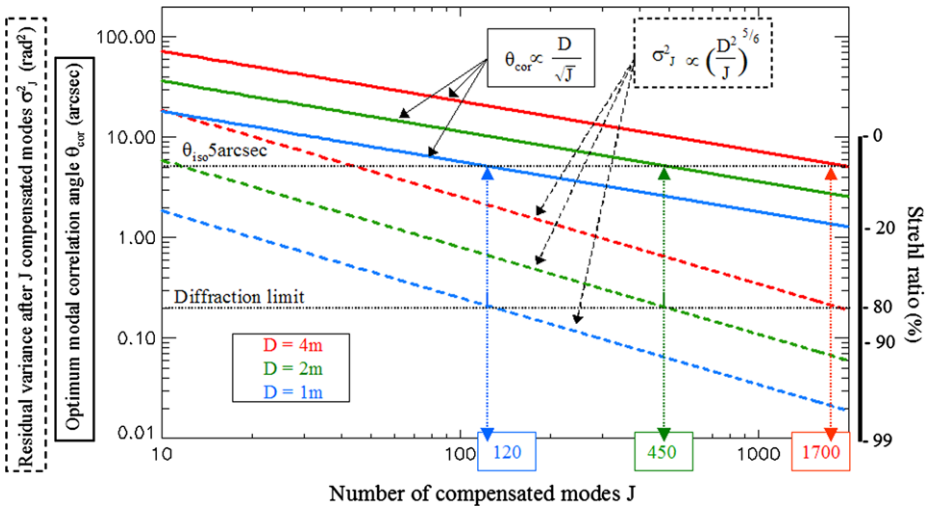
### 2.2. Determination of the Image Quality after AO Compensation

The statistical estimation of terrestrial turbulence effects is well suited to analyze long exposure data such as high-sensitivity spectropolarimetry observations. The acquisition time for diffraction-limited observations is longer than a few hundred milliseconds (a millisecond is the coherence time of the turbulence). We must use a criterion to evaluate the quality of the restored image. This criterion is based on the residual phase variance, which must be lower than a given value  $\sigma_J^2$  [rad<sup>2</sup>]. The residual phase variance has been approximated by Noll (1976) for a large number of corrected modes ( $J > 10$ ):

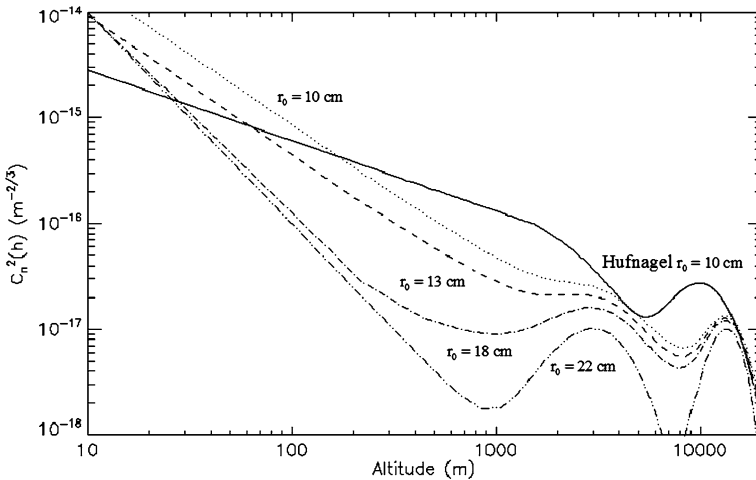
$$\sigma_J^2 = 0.2944 J^{-\frac{\sqrt{3}}{2}} \left( \frac{D}{r_0} \right)^{\frac{5}{3}} \quad \text{or} \quad \sigma_J^2 \propto \left( \frac{D^2}{J} \right)^{\frac{5}{6}}. \tag{14}$$

Figure 2 shows the optimal field of view [ $\theta_{\text{cor}}$ ] and the optimal image quality related to the residual phase variance [ $\sigma_J^2$ ] versus the number of compensated modes [ $J$ ] of the AO for three different telescope apertures (one-, two-, and four-meter telescopes). The dashed lower lines indicate the image quality expected after  $J$  compensated modes (the Strehl ratio is  $SR = \exp(-\sigma^2)$ ). For instance, the conventional diffraction-limited aberration level is set at a Strehl ratio of 0.8, i.e. a value of  $\sigma^2 = 0.2 \text{ rad}^2$  (indicated by the horizontal dotted line in Figure 2). Vertical arrows defined by the intersection of the 80% Strehl ratio and the  $\sigma_J^2$  functions give both the maximum order of compensated  $J$  of the AO and the isoplanatic domain, defined as twice the isoplanatic angle [intersection of the arrow and  $\theta_{\text{cor}}$  functions]. A  $\theta_{\text{iso}}$  of five arcseconds is found for the Hufnagel profile (Hufnagel, 1974) that has been used to calculate the different terms in the residual wavefront error (Figure 3).

We remark first that the isoplanatic domain at diffraction after AO compensation is independent of the telescope aperture. Second, for a four-meter class telescope, increasing the number of degrees of freedom [ $J$ ] from 450 to 1700 does not lead to a significant increase



**Figure 2** Optimal field of view  $[\theta_{cor}]$  (plain lines) and optimal image quality related to the residual phase variance  $[\sigma_J^2]$  (dashed lines) versus the number of compensated modes  $[J]$  of the AO for three different telescope apertures (one-, two-, and four-meter class telescopes respectively indicated in blue, green, and red). Vertical axis on left shows both the residual phase variance  $[\text{rad}^2]$  and the optimum field of view [arcseconds]. Right vertical axis indicates the Strehl ratio related to the residual phase variance. Notice that the conventional diffraction-limited aberration level is set at a Strehl ratio of 0.8, i.e. a value of  $\sigma^2 = 0.2 \text{ rad}^2$ .



**Figure 3** Plots of  $C_n^2$  turbulence profiles from analytical modeling ( $r_0 = 10 \text{ cm}$  at  $\lambda = 0.5 \mu\text{m}$ ) suggested by Hufnagel in comparison with  $C_n^2$  profiles from experimental measurements at Izaña in the Canary Islands. The profiles are integrated from 10 m (above the ground) to 20 000 m to give Fried's parameter  $r_0$  at  $\lambda = 0.5 \mu\text{m}$  from 10 cm to 22 cm.

of the Strehl ratio but reduces by 66% the useful field of view. In the following, we refine the analytical model especially for a low-order AO system to determine the largest isoplanatic field of view. The residual wavefront distortions can be described modally in terms of Zernike polynomials. The latter are chosen for their simple analytical form, and because of

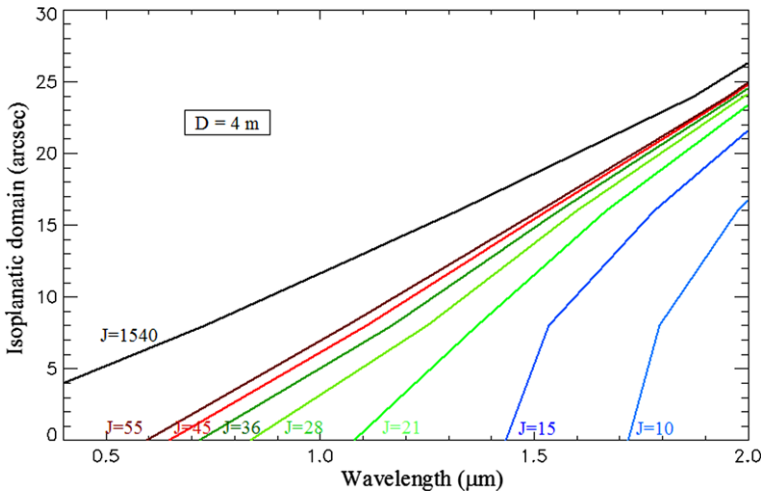


**Figure 4** Isoplanatic domain (twice the isoplanatic angle  $\theta_{iso}$ ) corresponding to an image quality criterion of  $\lambda/5$  versus wavelength, for a four-meter class telescope after compensation of  $J = 10$  to 1540 modes. Curves are computed with the Hufnagel  $C_n^2$  turbulence profile ( $r_0 = 10$  cm at  $\lambda = 0.5 \mu\text{m}$ ).

the correspondence of the low-order Zernike polynomials to physically controllable modes of correction (e.g., tilt, focus, and astigmatism). For instance, an AO system compensating for turbulence disturbances up to the maximum radial degree  $N$  ( $N = 1$  for tip-tilt system) on an astronomical source at an angle  $\alpha$  from the AO source reference is characterized by the residual variance

$$\sigma^2(N, \alpha) = \left(\frac{D}{r_0(\lambda)}\right)^{5/3} f(N, \alpha), \tag{15}$$

where  $D$  is the telescope diameter,  $r_0(\lambda)$  at wavelength  $\lambda$  is the Fried parameter, and  $f(N, \alpha)$  is the function expressed analytically by Equation (32) of Appendix A.

The isoplanatic angle  $[\alpha_{iso}]$  is given by the equality

$$\left(\frac{D}{r_0(\lambda)}\right)^{5/3} f(N, \alpha_{iso}) = \sigma_0^2 = \left(\frac{2\pi}{a}\right)^2 [\text{rad}^2] \tag{16}$$

where the standard deviation  $\Delta_{sd} = \sqrt{\sigma_0^2}$  is expressed in wavelength units:  $\Delta_{sd} = \lambda/a$  (rms). Using the relation between the wavelength and the residual phase variance, Equation (16) can be written as

$$\lambda (\mu\text{m}) = \frac{a}{2\pi} \sqrt{f(\alpha_{iso})} 0.5 \left(\frac{D}{r_0(\lambda)}\right)^{5/6} \tag{17}$$

where  $r_0$  is the Fried parameter calculated at the wavelength  $\lambda = 0.5 \mu\text{m}$ .

Figure 4 gives the isoplanatic domain (twice the defined isoplanatic angle  $\alpha_{iso}$ ) for  $\sigma_0 = 2\pi/5$  corresponding to  $\lambda/5$ , i.e. a Strehl ratio of about 20%. This arbitrary value of the residual error is the minimum image quality expected for astronomical observations. Figure 4 shows the isoplanatic domains estimated for a four-meter class telescope after compensation by different adaptive systems from a low-order system after  $J = 10$  corrected modes to  $J = 1540$  to reach the diffraction limit in the visible wavelength range. Figure 5

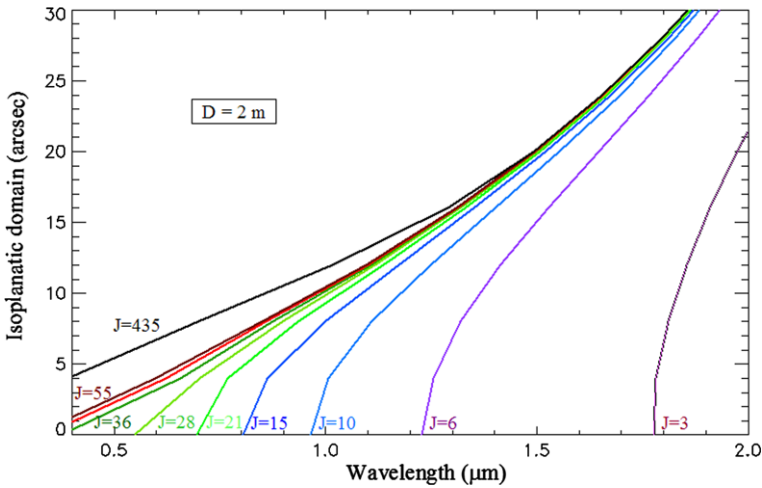


**Figure 5** Isoplanatic domain (twice the isoplanatic angle  $\theta_{iso}$ ) corresponding to an image-quality criterion of  $\lambda/5$  versus wavelength, for a two-meter class telescope after compensation of  $J = 10$  to 435 modes. Curves are computed with the Hufnagel  $C_n^2$  turbulence profile ( $r_0 = 10$  cm at  $\lambda = 0.5 \mu\text{m}$ ).

shows the isoplanatic domain estimated for a two-meter class telescope after compensation from  $J = 10$  corrected modes up to  $J = 435$  modes. We show that the capacity of a high-order AO system is suitable for high spatial resolution observations with a severe reduction of the field of view. As expected, the isoplanatic angle  $[\alpha_{iso}]$  increases with wavelength. A four-meter class telescope would be well sized to the study of magnetic-field dynamics at the granule scale. A question remains as to the adequacy of a four-meter class as compared to a two-meter class telescope except for the purpose of collecting more photons.

We have examined the daytime measurements of  $r_0$  from balloon-sonde measurements performed for several months (Barletti *et al.*, 1973). The daytime data contain a number of high values of  $r_0$ , which are mostly from the very early morning, when the air is still quite stable. However, the measurements of  $r_0$  must be corrected for the zenith angle of the Sun to get a true estimate of what the solar observation would be like. If  $r_0$  is measured as 15 cm at the Zenith, then for the Sun observed at ten degrees above the horizon, the effective  $r_0$  would be around 6 cm. Table 1 shows the estimated values of the isoplanatic angle for different observation conditions measured at Izaña in the Canary Islands corresponding to the turbulence profiles displayed in Figure 3. The corresponding percentage of  $r_0$  is deduced from the exceedance probability function. For each case, the required number of AO actuators to reach the diffraction limit with a four-meter-aperture class telescope at  $0.5 \mu\text{m}$  is indicated. Note that, at an equivalent Fried parameter ( $r_0 = 10$  cm), the isoplanatic angle derived with the Izaña model is smaller than the Hufnagel one. This is due to the unfavorable contribution of layers distributed in altitude.

The residual variance of Equation (15) depends on the ratio  $[D/r_0(\lambda)]^{5/3}$ . The Fried parameter depends on the wavelength and the turbulence profile considered:

$$r_0(\lambda) = \left[ \frac{0.033(2\pi)^{-2/3}k^2}{0.023 \cos \gamma} \int_0^{L_{atm}} dh C_n^2(h) \right]^{-3/5} \propto \lambda^{6/5}, \tag{18}$$

where  $\gamma$  is the angle to Zenith, and  $C_n^2(h)$  the turbulence profile.

**Table 1** Estimation of the isoplanatic angle  $[\theta_{\text{iso}}]$  and the minimum AO number of actuators (necessary to reach the diffraction with a four-meter-aperture class telescope in the visible wavelength range) for different observation conditions [%] corresponding to the  $C_n^2$  profiles derived from experimental measurements at Izaña in the Canary Islands. The profiles are integrated from 10 m (above the ground) to 20 000 m to give Fried’s parameter  $r_0$  at  $\lambda = 0.5 \mu\text{m}$  from 10 cm to 22 cm.

| Profile  | Probability [%] | Fried parameter [cm] | Number of actuators | $\theta_{\text{iso}}$ [arcseconds] |
|----------|-----------------|----------------------|---------------------|------------------------------------|
| Hufnagel | –               | 10                   | 1300                | 5                                  |
| Izaña    | 50              | 10                   | 1300                | 4                                  |
| Izaña    | 10              | 18                   | 500                 | 10                                 |
| Izaña    | 2               | 22                   | 350                 | 13                                 |

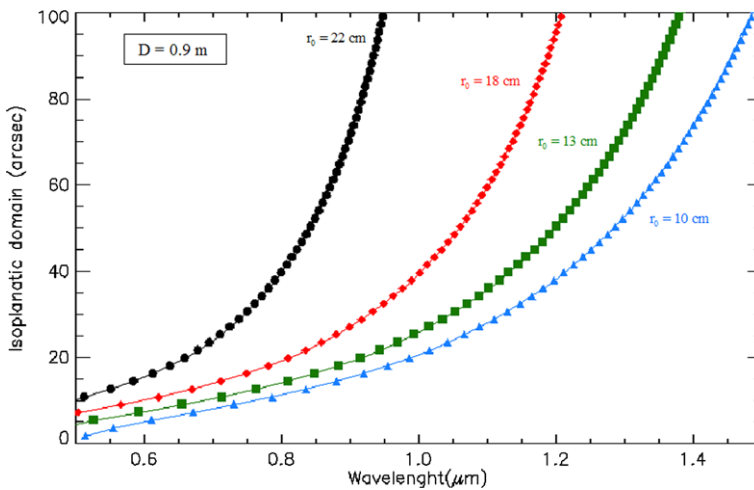


**Figure 6** Isoplanatic domain (twice the isoplanatic angle  $\theta_{\text{iso}}$ ) corresponding to an image-quality criterion of  $\lambda/5$  versus wavelength, for a one-meter class telescope after compensation of  $J = 10$  modes. Curves are calculated with the modeled profile at Izaña ( $D/r_0 = 4$  to 10).

For instance, the performance of a one-meter class telescope observing in the visible wavelength range at  $\lambda = 0.5 \mu\text{m}$  is equivalent to the performance obtained with a four-meter class telescope in the infrared range at  $\lambda = 1.6 \mu\text{m}$ .

Considering that a large field of view after AO compensation is a crucial requirement for extrapolation of the magnetic-field studies, a one-meter class telescope using a low-order AO system would be an interesting compromise for observations in the infrared wavelength range. This point of view is emphasized in Figure 6, where we consider isoplanatic domains after low-order AO system compensation ( $J = 10$ ) for different values of the Fried parameter  $r_0$  determined from experimental measurements at Izaña (Barletti *et al.*, 1973).

### 3. Spectropolarimetry Issues

#### 3.1. The Magnetic Flux Measurements

We analyzed spectra obtained from high spatial resolution observations obtained with a ground-based long-slit spectrograph to determine the specific requirements of magnetog-

raphy. Even though focused studies of small  $\delta$ -spots require only relatively small fields of views, about 1.6 arcminutes (Canou *et al.*, 2009), the typical field of view required for extrapolation purposes is larger than two arcminutes: typically three to four arcminutes for emerging active regions, sigmoids, and medium-sized filaments (Aulanier and Schmieder, 2002; Pariat *et al.*, 2004; Schrijver *et al.*, 2008; Canou and Amari, 2010), and up to six arcminutes for large filaments and full AR studies (Lionello *et al.*, 2002; Metcalf *et al.*, 2008; Masson *et al.*, 2009). It would be a major observational leap forward on flare and coronal mass ejection research, *via* photospheric–chromospheric vector magnetic-field maps accompanied by magnetic-field extrapolations, to have direct observation of the lower atmospheric trace of coronal current sheets. These current sheets are the key ingredient for magnetic reconnection (both in the seminal Sweet–Parker and Petscheck models, as well as in more recent collisionless reconnection models), which powers flares. Magnetohydrodynamic (MHD) theory states that these current sheets should extend all along the three-dimensional (quasi)separatrix surfaces (which separate regions of distinct magnetic field connectivities), and not only at the reconnection site (Low and Wolfson, 1988; Masson *et al.*, 2009; Moreno-Insertis, Galsgaard, and Ugarte-Urra, 2009). Observing the low atmospheric trace of such sheets requires a high-resolution combined with a high polarimetric sensitivity, so as to measure small-scale changes in the amplitude and direction of horizontal fields (*via* Ampere’s law). Second, various MHD models also invoke the occurrence of current sheets and reconnection right in the photo–chromosphere, *e.g.* for of buildup of active-region scale, more-or-less twisted-fields that can eventually erupt (Van Ballegooyen and Martens, 1989; Aulanier *et al.*, 2010), or during flux emergence for the gradual formation of classical  $\Omega$ -loops (Pariat *et al.*, 2004; Archontis and Hood, 2009; Cheung *et al.*, 2010). Until now, those currents have only been obtained from MHD simulation; their real observational existence is not yet proven. For both cases, one needs to observe the full active-region field of view to catch the current sheets, because their exact location is hard to predict within an active region, and because their use for subsequent full active region scale modeling requires a homogeneous magnetogram.

As a reference, we use a magnetic field map, derived from spectropolarimetric observations made with the ground-based THEMIS telescope. The one-meter class magnetograph was designed to obtain 0.45 arcsecond spatial resolution measurements in the visible wavelength range of the solar magnetic-field vector from simultaneous observations of different polarized spectral lines (Bommier *et al.*, 2007). Figure 7 displays a comparison between SOHO/MDI (at high spatial resolution, 0.6 arcsecond) and THEMIS/MTR of the same active region (AR) 8668. The observation from THEMIS consists of several successive steps of the slit scanning along a direction perpendicular to it, which results in a two-dimensional spatial map (100 steps of a scan of the 0.4 arcsecond by 100 arcseconds slit). Spectra are separated by 0.8 arcsecond, and the exposure time per frame is 0.3 second. A scan of the region ( $160 \times 110$  arcseconds<sup>2</sup>) took 35 minutes for ten spectral domains and the Stokes sequence ( $Q, U, V$ ). The THEMIS map shows a better spatial resolution than that of SOHO in both directions (0.4 arcsec). Nevertheless, the filling factor is changing due to the imprecise position of the slit throughout the scan: weak vertical strips are perceptible.

### 3.2. The Infrared Spectral Domain Alternative

The near-infrared spectral domain remains the only possibility to obtain a large field of view using a classical adaptive optics (AO) system for a four-meter class telescope. Examples are the COMEon + 52-actuator (Léna, 1994) or the NAOS 185-actuator system (Lagrange *et al.*, 2003). Two phenomena confer a serious advantage to choosing the infrared spectral domain

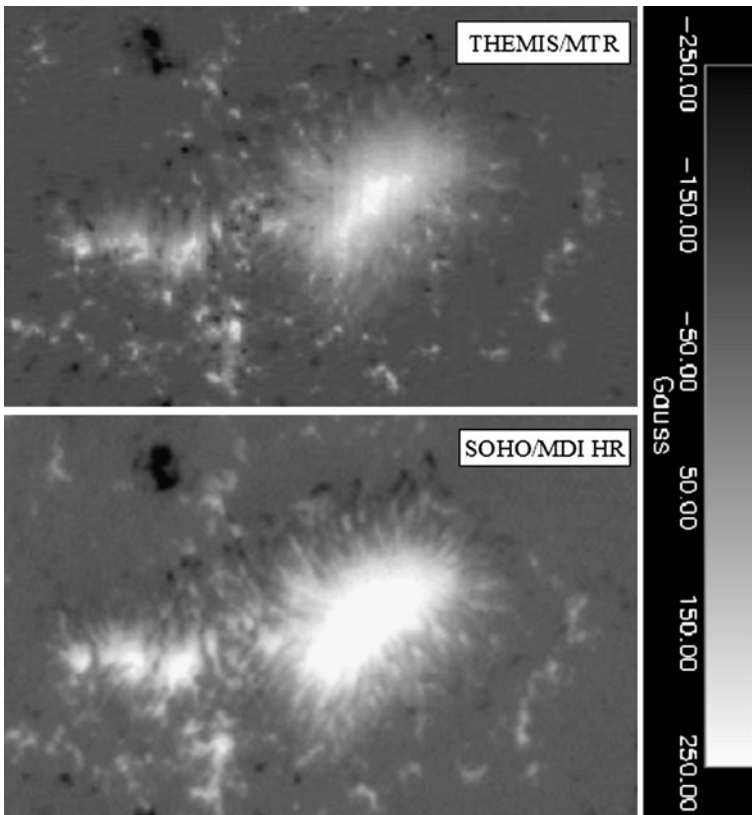


**Figure 7** Magnetic flux maps of AR 8668 observed 20 August 1999 with SOHO/MDI at high resolution at 0819 UT and with THEMIS at 0849 UT. Below: SOHO/MDI; the pixel resolution is 0.6 arcsecond. Above: THEMIS; 100 steps of a 0.4 arcsecond by 100 arcseconds slit scan is displayed. The separation between spectra is 0.8 arcsecond, and the exposure time per frame is 0.3 second.

for magnetometry for large-aperture telescopes. The first is due to the higher sensitivity of the infrared spectral lines to the Zeeman effect: Zeeman shifts are proportional to  $g\lambda^2$  where  $g$  is the Landé factor. The second comes from the properties of the turbulence: the value of Fried's parameter  $r_0 = 10$  cm in the visible wavelength range becomes 60 cm at  $2.2 \mu\text{m}$ , for instance. Figure 8 shows that the expected isoplanatic field of view is four times larger in the  $1.6 \mu\text{m}$  infrared than in the visible range.

Table 2 shows the estimated values of the isoplanatic angle for different observation conditions presented in Table 1. For each case, the required number of AO-system actuators to reach the diffraction limit with a four-meter-aperture class telescope in the infrared wavelength range ( $1.6 \mu\text{m}$ ) is indicated.

### 3.3. The Low-Order AO System Alternative

Accurate magnetic-field topology studies require first of all a homogeneous spatial resolution over an extended field of view. In the following, we explore the ability of a low-order AO system that allows one to obtain the largest homogeneous field of view at a lower spatial resolution. For that purpose, we select the minimum AO case of only ten compensated

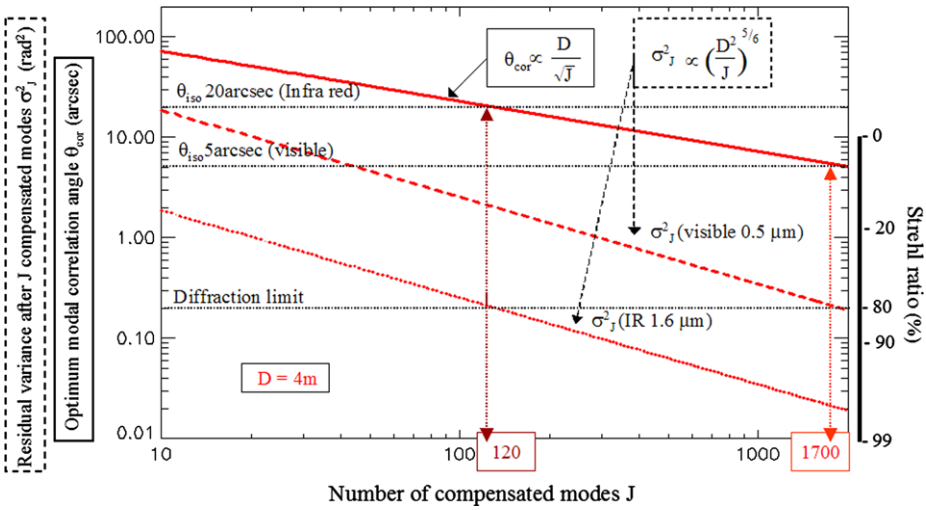


**Figure 8** Comparison of the optimal field of view [ $\theta_{cor}$ ] (plain lines) and optimal image quality related to the residual phase variance [ $\sigma_J^2$ ] (dashed lines) versus the number of compensated modes [ $J$ ] of the AO for the visible and the infrared spectral domains (four-meter class telescope). Vertical axis on left shows both the residual phase variance [ $\text{rad}^2$ ] and the optimum field of view [arcseconds]. Right vertical axis indicates the Strehl ratio related to the residual phase variance.

**Table 2** Estimation of the isoplanatic angle [ $\theta_{iso}$ ] and the minimum AO number of actuators (necessary to reach the diffraction limit with a four-meter-aperture class telescope in the infrared wavelength, at  $1.6 \mu\text{m}$ ) for different observation conditions [%] and corresponding to the  $C_n^2$  profiles derived from experimental measurements at Izaña in the Canary Islands. The profiles are integrated from 10 m (above the ground) to 20 000 m to give Fried’s parameter  $r_0$  at  $\lambda = 1.6 \mu\text{m}$  from 40 cm to 89 cm.

| Profile  | Probability [%] | Fried parameter [cm] | Number of actuators | $\theta_{iso}$ [arcseconds] |
|----------|-----------------|----------------------|---------------------|-----------------------------|
| Hufnagel | –               | 40                   | 120                 | 20                          |
| Izaña    | 50              | 40                   | 120                 | 18                          |
| Izaña    | 10              | 72.5                 | 35                  | 30                          |
| Izaña    | 2               | 89                   | 25                  | 35                          |

modes to show the interest of the low-order system in favorable observation conditions (less than a few percent of the time) in the near-infrared spectral band ( $1.6 \mu\text{m}$ ) for a four-meter class telescope. The performance is the same as that of a one-meter class telescope in the visible region, as indicated by Equation (18).

We analyze the nonlinear degradation of the magnetic-field measurements obtained with a long-slit spectrograph system on a large field of view, taking into account the effects of anisoplanatism of terrestrial turbulence. The technique to simulate the optical transfer functions (OTFs) is described in detail in Appendix B. The effects of anisoplanatism are presented in Figure 9 for excellent observation conditions at Izaña (less than 2% of the time and corresponding to  $D/r_0 = 5$ ). The OTF after compensation through tip-tilt ( $J = 3$ ), astigmatism ( $J = 6$ ), and coma ( $J = 10$ ) are displayed for different angular separations in the field of view for the same turbulence profile. As expected, one observes that the image-quality improvement, when compensating ten modes, decreases rapidly when the angular

separation increases for an extended source. At very large angles ( $\alpha \geq 20$  arcseconds) in Figure 9, the image quality after compensation of ten modes for  $D/r_0 = 5$  is hardly better than that obtained without correction, because of the wavefront angular decorrelation. Figure 10 shows a comparison of the effects of anisoplanatism on a magnetic-field map after real-time compensation by an image-stabilizer system, and by a ten controllable-modes AO system in excellent observation conditions – less than 2% of the time at Izaña (Barletti *et al.*, 1973). We show the significant improvement of the spatial resolution, for observations in the near-infrared wavelength range, when compensating the first ten aberration modes at the field-of-view center. In this configuration, the AO system is centered on the sunspot, and anisoplanatism effects are equivalent in both directions (parallel, and perpendicular to the scan). This will not be the case of a hypothetical AO system working together with the scan, *i.e.*, in a stop-and-go synchronization for each scanning step (more difficult to do).

In this simulation, a comparison of the retrieved shape of the magnetic-flux density profile along the horizontal direction at the center of the maps after compensation demonstrates the necessity of obtaining a homogeneous field of view with regard to the spatial resolution. Spectroscopic diagnostics of the magnetic field require one to compensate for motions coming from instrument vibrations and guiding errors as well as from random wavefront motions caused by terrestrial atmospheric turbulence. Figure 11 presents a quantitative evaluation of the spatial resolution after compensation by the system for a four-meter class telescope in the near-infrared wavelength range. One observes a significant increase of anisoplanatism effects in the field of view with the increase in the number of corrected modes. This simulation allows us to understand that for small field-of-view observations, compensation of the maximum of aberration modes is the best choice in terms of image quality, keeping in mind the rapid degradation of this quality in the field of view. By contrast, with a low-order system compensation, the image quality does not vary rapidly with the field angle. It also reveals the important contribution of the large isoplanatic domain of the tip-tilt aberrations for AO compensation. At a very large angle ( $\alpha \geq 20$  arcseconds), with  $D/r_0 = 5$ , the correction by a stabilizer system is even better than that obtained with the compensation of the first ten aberration modes by an AO system. For a four-meter class telescope, the on-axis correction is relatively good considering the evaluation of the Fried resolution (0.32 arcsecond in the central part of the field of view), and the degradation does not vary rapidly with the field angle. This is due to the dominant contribution of the lowest altitude layers in the angular correlation of the wavefronts. By comparison, the ten corrected-modes AO system is the best choice in terms of image quality, keeping in mind the rapid degradation of the quality in the field (resolution of 0.18 arcsecond up to 0.5 arcsecond in the 2 arcminutes<sup>2</sup> field of view). This demonstrates the importance of the decorrelation of the higher wavefront-deformation modes in the field.

Accurate magnetic-field topology studies require a homogeneous spatial resolution over an extended field of view. Classical low-order AO systems can achieve the required performance in the near-infrared wavelength range under routine observation conditions. Examples for night-time observations are the COMEon + 52-actuator (Léna, 1994) or the NAOS 185-actuator system (Lagrange *et al.*, 2003). Recently, the New Solar Telescope (NST), the 1.6 m clear aperture at the Big Bear Solar Observatory (BBSO) is providing high-resolution two-dimensional spectroscopic and polarimetric imaging in the near infrared region. The 308 sub-aperture (349-actuator deformable mirror) AO system will enable nearly diffraction-limited observations at 1.7  $\mu\text{m}$ . (Cao *et al.*, 2010).

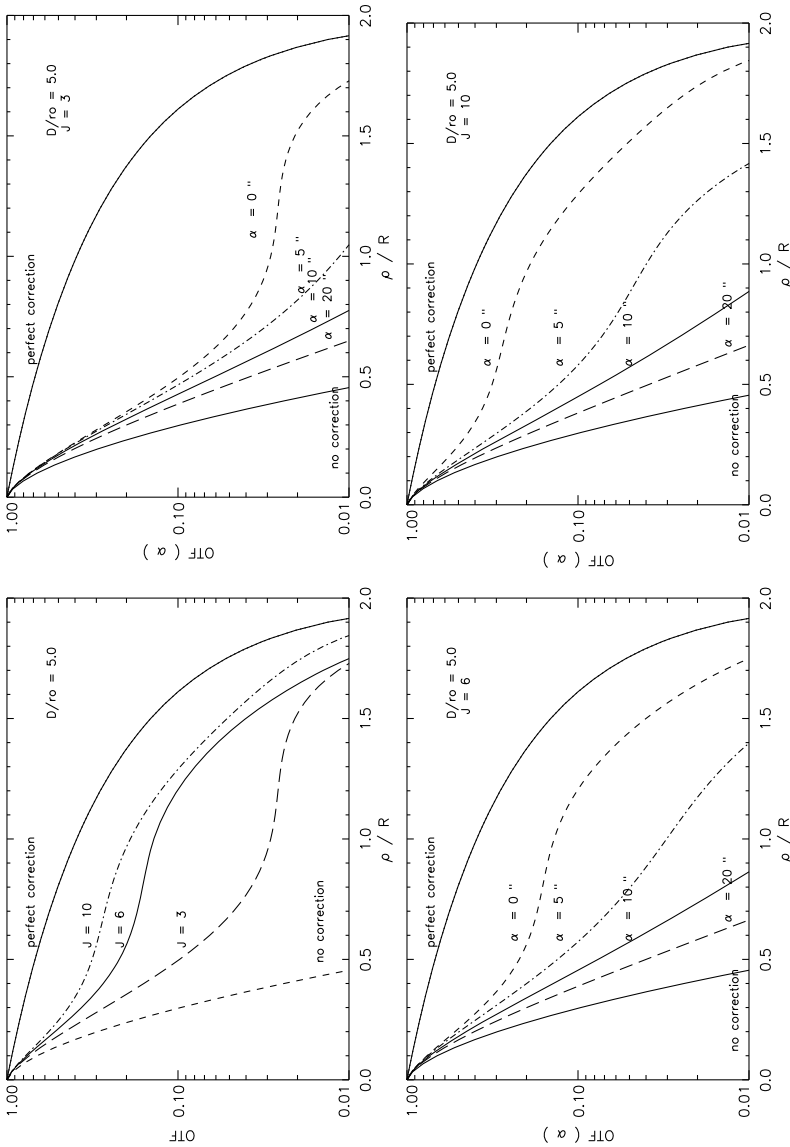


**Figure 9** OTF versus the normalized spatial frequency  $[\rho/R]$ . Top left: OTF on-axis computed for modal compensation up to the mode  $J$ . Top right: OTF( $\alpha$ ) after tip-tilt correction ( $J = 3$ ) for several angular separations  $[\alpha]$ , and a ratio of  $D/r_0 = 5$  ( $D$  being the telescope aperture, and  $r_0$  the Fried parameter). Bottom left: OTF( $\alpha$ ) after compensation of tip-tilt, defocus, and astigmatism, and bottom right: after compensation of modes through the coma [ $J = 10$ ]. The full curve is diffraction limited;  $\rho/R = 2$  corresponds to the diffraction limit.

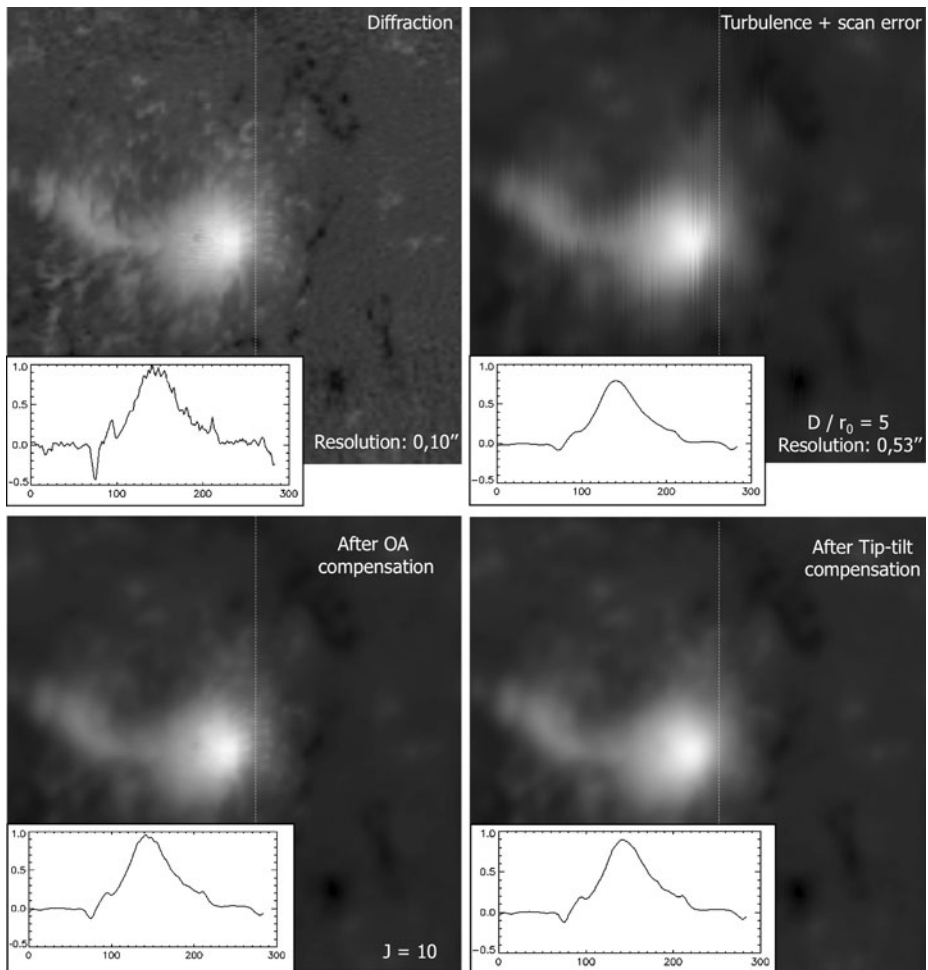


**Figure 10** Top left: Magnetic map observed with THEMIS, 17 August 1999, and selected as the reference map for the simulation at the diffraction limit (the spatial resolution would be, for example, 0.1 arcsecond at  $\lambda = 1.6 \mu\text{m}$  for a four-meter class telescope). The size of the field of view (for the purpose of the simulation) is  $2 \times 2$  arcminutes<sup>2</sup>. Top right: Effects of the turbulence and instrumental motions for a long-time exposure ( $D/r_0 = 5$ ). The spatial resolution is five times the diffraction limit (for example, around 0.53 arcsecond at  $\lambda = 1.6 \mu\text{m}$  for a four-meter-aperture telescope). Bottom left: Anisoplanatism effects after real-time compensation by the AO at the FOV center of ten controllable modes (tip-tilt, focus, astigmatism, and coma). Bottom right: Anisoplanatism effects after tip-tilt compensation at the FOV center by the system. The intensity of the magnetic field along the horizontal direction at the center of the image is indicated for each case.

#### 4. Conclusion

We have presented a study to evaluate the adaptive optics (AO) system limitations in regard to the scientific requirements expected for magnetic-field extrapolations, and data-driven magnetohydrodynamic (MHD) simulations of large fields of view. Questions we have addressed include: Can ground-based telescopes with AO systems fulfill the requirements of extrapolations and data-driven MHD simulations? In other words, are large fields of view a few arcminutes in size accessible at high spatial resolution from the ground? Irrespective

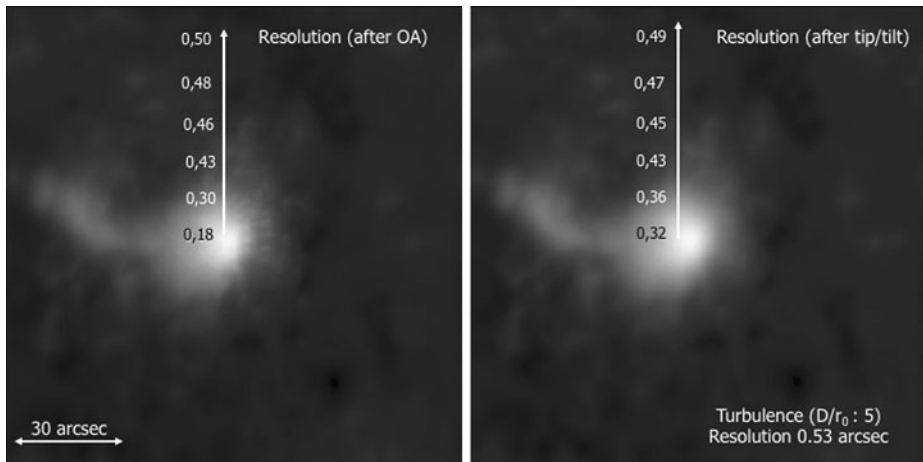


**Figure 11** Evaluation of the Fried resolution in the field of view ( $2 \times 2$  arcminutes<sup>2</sup>) after tip–tilt compensation (right), and (left) for a low-order AO system after correction of ten controllable modes (tip–tilt, focus, astigmatism, and coma). Spatial resolution indicated is derived in the case of a four-meter class telescope at  $\lambda = 1.6 \mu\text{m}$ . By comparison, the resolution without correction is only 0.53 arcsecond ( $r_0 = 72$  cm).

of the science goals associated with small fields of view (*e.g.*, magnetic field and plasma dynamics of the network, the interwork, or sunspot penumbrae), reliable, regular magnetic-field measurements at active-region-scale (several arcminutes wide) fields of view are indeed most relevant for investigations on flares, and on CME triggering and development, which are part of the growing effort in understanding space weather. Based on the seminal work by Hufnagel as well as measurements based on atmospheric-turbulence profiles, we show first that the visible-wavelength domain still remains difficult to explore with a ground-based telescope using a classical AO system. The isoplanatic field of view resulting from the compensation of a classic AO system is only a few arcseconds at the diffraction limit for typical conditions of atmospheric turbulence, *i.e.*  $r_0 = 10$  cm, which occur more than 50% of the time in solar observatories. The field of view does not reach more than 13 arcseconds for exceptional values of  $r_0 = 22$  cm, which are known to occur no more than 2% of the time. These figures, in addition to the well-known degradation of the spatial resolution away from the isoplanatic domain with AO, seem to be incompatible with reaching multi-arcminute active-region-scale fields of view.

The problem of anisoplanatism is already known to be the major difficulty for observations of extended sources (Sanakarasubramanian and Rimmele, 2008). The classical AO system is unable to reach the required performances in the visible wavelength range under normal observation conditions. A new generation of AO systems such as multiconjugate adaptive optics (MCAO) systems (Langlois *et al.*, 2004) must be envisaged to expect larger fields of view. Due to its extended nature, the Sun is an ideal object for which to develop MCAO techniques; they become a priority in overcoming the severe limitation of conventional AO systems (Rimmele, 2006; Berkefeld, 2006; Rimmele *et al.*, 2010). Wide-field adaptive optics has been demonstrated recently in the laboratory in view of an implementation on a real system for night-time observations (Costille *et al.*, 2010). A challenging new approach called multi-object adaptive optics (MOAO) has been recently demonstrated for night-time observations with a deformable mirror driven open-loop, and controlled through a tomographic reconstruction by three guide stars (Gen-

dron *et al.*, 2011). Nevertheless, to the authors' knowledge, there is no MCAO system working routinely on the sky at this time.

Second, we show that the infrared spectral domain remains the only possibility to obtain large fields of view using classical AO systems for large-aperture telescopes. One noticeable advantage comes from the higher sensitivity of the IR spectral lines to determine the magnetic flux from spectropolarimetric observations with ground-based observations at 1.56  $\mu\text{m}$  (Beck and Rezaei, 2009) and at 1.083 He I (Kuckein, Centeno, and Martinez Pillet, 2010) to study chromospheric dynamics.

For a classical AO system, it has been shown that the best image quality is obtained by limiting the system correction capabilities to an adequate number of spatial modes (Gendron and Léna, 1994). The expected isoplanatic field of view at diffraction is four times larger in the 1.6  $\mu\text{m}$  IR band than in the visible range (*i.e.*, 20 instead of 5 arcseconds) for usual conditions of observation ( $r_0 = 10$  cm), but it still remains far too small to cover a whole active region in a single scan. Exceptional turbulence conditions with  $r_0 = 22$  cm, which occur 2% of the time at best, increase this field of view up to 35 arcseconds. This is still too small to tackle the multi-arcminute field-of-view cases listed in Section 1, but it now allows for the study of small ephemeral active regions. Achieving mosaics from multiple scan passages may be an answer to obtaining active-region-scale multi-arcminute fields of view. The feasibility of this challenging observational protocol for spectropolarimetry is yet to be demonstrated on large aperture solar telescopes with AO systems.

**Acknowledgements** We are grateful to the referees, who helped us in addressing many potential counter-arguments which could be raised against the results obtained in this study. Simulations are based on observations made with the French–Italian THEMIS telescope operated by CNRS and CNR on the island of Tenerife at the Spanish Observatorio del Teide of the Instituto de Astrofísica de Canarias.

## Appendix A: Derivation of the Residual Wavefront Error

New techniques to simulate effects of anisoplanatism based on image reconstruction have been recently proposed (Aubailly, Roggeman, and Schultz, 2007). In order to evaluate the limitations due to anisoplanatism, we adopted a theoretical analysis based on the modal control of the adaptive optics (AO) system. Modal control is a helpful tool in AO to manage optimal correction in terms of temporal and angular decorrelation of turbulent wavefronts. We use the Mellin transform technique to evaluate the effects of anisoplanatism on the performance of AO systems (Chassat, 1989; Sasiela, 1988; Molodij and Rousset, 1997; Molodij and Rayrole, 1998; Molodij, 2011). We derive the optical transfer functions (OTFs) to evaluate the degradation in the field of view due to anisoplanatism after AO compensation. The OTFs are evaluated for a Zernike expansion following the Wang and Markey (1978) approach. The statistics of the Zernike coefficients for an expansion of Kolmogorov turbulence phase distortion were derived by Noll (1976) and applied to calculate the OTFs for a point source (Wang and Markey, 1978). In order to determine the compensation quality in a field of view, the residual phase variance over the telescope aperture is expressed expanding the turbulent wavefront on the Zernike polynomials (or modes). The properties of Zernike polynomials  $[Z_j]$  are well described by Noll (1976), whose notation is adopted. The wavefront  $\phi(\mathbf{r}, \alpha)$  incoming from a determined area on the Sun, located at angular distance  $\alpha$  from the on-axis observed direction, is expanded as (piston mode removed)

$$\phi(R\mathbf{u}, \alpha) = \sum_{j=2}^{\infty} a_j(\alpha) Z_j(\mathbf{u}), \quad (19)$$

where  $\mathbf{u}$  is the normalized position vector in the aperture,  $R$  the radius of the telescope aperture, and the  $a_j(\alpha)$  the Zernike expansion coefficients given by

$$a_j(\alpha) = \int d^2\mathbf{u} W(\mathbf{u})\phi(R\mathbf{u}, \alpha)Z_j(\mathbf{u}), \tag{20}$$

introducing the Noll normalization function:

$$W(\mathbf{u}) = \begin{cases} \frac{1}{\pi}: & \text{if } |\mathbf{u}| \leq 1, \\ 0: & \text{elsewhere.} \end{cases} \tag{21}$$

So, the polynomials  $Z_j(\mathbf{u})$  normalized over the telescope aperture are defined in polar coordinates  $(u, \theta)$  by

$$Z_j(u, \theta) = \sqrt{n+1} \begin{cases} R_n^m(u)\sqrt{2}\cos(m\theta) : & \text{if } j \text{ even, and } m \neq 0, \\ R_n^m(u)\sqrt{2}\sin(m\theta) : & \text{if } j \text{ odd, and } m \neq 0, \\ R_n^0(u) : & \text{if } m = 0 \end{cases} \tag{22}$$

and

$$R_n^m(u) = \sum_{s=0}^{\frac{n-m}{2}} \frac{(-1)^s (n-s)!}{s! [\frac{n+m}{2} - s]! [\frac{n-m}{2} - s]!} u^{n-2s}, \tag{23}$$

where  $n$  is the radial degree of the  $j$ th polynomial, and  $m$  its azimuthal frequency.

Let  $\hat{\phi}(R\mathbf{u})$  be the estimated wavefront reconstructed by the AO system on the first  $J$  polynomials from the measurements. In this article, noise in the wavefront measurement is not considered; therefore, we write:

$$\hat{\phi}(R\mathbf{u}) = \sum_{j=2}^J a_j Z_j(\mathbf{u}). \tag{24}$$

The residual phase variance  $\sigma^2(J, \alpha)$  is estimated for an AO system having  $J$  degrees of freedom, and for an angular distance  $\alpha$  between the two directions:

$$\sigma^2(J, \alpha) = \int d^2\mathbf{u} W(\mathbf{u}) \langle (\phi(R\mathbf{u}, \alpha) - \hat{\phi}(R\mathbf{u}))^2 \rangle. \tag{25}$$

Using the orthogonality properties of Zernike polynomials, Equation (19) and Equation (24), and the stationarity hypothesis, the residual phase variance is

$$\sigma^2(J, \alpha) = \sum_{j=J+1}^{\infty} \langle (a_j)^2 \rangle + 2 \sum_{j=2}^J [\langle (a_j)^2 \rangle - \langle a_j(\alpha)a_j(0) \rangle]. \tag{26}$$

This result is classical in the estimation of wavefront residual error on the Zernike polynomial (Chassat, 1989; Rousset, 1993; Molodij and Rayrole, 1998). We recognize the first term as the fitting error when the AO system corrects the first  $J$  polynomials. It has been given by Noll (1976). The other term on the right-hand side of Equation (26) is the spatial and angular wavefront error.

The residual error can be written as

$$\sigma^2(J, \alpha) = \sum_{j=2}^{\infty} \langle (a_j)^2 \rangle - \sum_{j=2}^J \underbrace{[2\langle a_j(\alpha)a_j(0) \rangle - \langle (a_j)^2 \rangle]}_{A(j, \alpha)}. \tag{27}$$

The quantity  $A(j, \alpha)$  is the spatial and angular error for the corrected polynomial  $Z_j$ . Correction by the AO system will be effective when  $A(j, \alpha)$  is greater than zero for each polynomial  $Z_j$ , *i.e.* when

$$\frac{\langle a_j(\alpha)a_j(0) \rangle}{\langle (a_j)^2 \rangle} \geq 0.5 \tag{28}$$

Now, the Zernike coefficient angular correlations  $[\langle a_j(\alpha)a_j(0) \rangle]$  between the two wavefront directions can be derived as indicated in Valley and Wandzura (1979), Chassat (1989), Molodij and Rousset (1997), Molodij and Rayrole (1998). Therefore, the Zernike coefficient angular correlation can be written as

$$\langle a_j(\alpha)a_j(0) \rangle = 3.895(n + 1) \left(\frac{D}{r_0}\right)^{\frac{5}{3}} \frac{\int_0^{L_{atm}} dh C_n^2(h) I_{n,m}(\frac{\alpha h}{R})}{\int_0^{L_{atm}} dh C_n^2(h)}, \tag{29}$$

where  $r_0$  is the Fried parameter,  $D$  the telescope diameter [ $D = 2R$ ],  $C_n^2$  the turbulence profile,  $h$  the altitude along the propagation path from the Sun to the telescope, and using the notation  $x = \frac{\alpha h}{R}$ ,

$$I_{n,m}(x) = s_{n,m} \int_0^{\infty} dK K^{-\frac{14}{3}} J_{n+1}^2(K) [J_0(Kx) + k_j J_{2m}(Kx)], \tag{30}$$

with

$$k_j = \begin{cases} 0: & \text{if } m = 0, \\ (-1)^j: & \text{if } m \neq 0, \end{cases}$$

$$s_{n,m} = \begin{cases} 1: & \text{if } m = 0, \\ (-1)^{(n-m)}: & \text{if } m \neq 0, \end{cases} \tag{31}$$

where  $K$  is the Fourier space of the Zernike polynomials in polar coordinates (Noll, 1976).

To calculate the residual phase variance of Equation (26), we consider first that the number  $[J]$  of corrected polynomials is chosen so as to include all the polynomials of the maximum radial degree  $[N]$ . Knowing that there are  $n + 1$  polynomials per radial degree  $n$ , we therefore have  $J = \frac{(N+1)(N+2)}{2}$ .

Second, the azimuthal-frequency symmetry properties of Zernike coefficient correlations are useful. Summation over all azimuthal frequencies of a radial degree leads to only a radial-degree dependence. Then, using Equation (29),

$$\sigma^2(N, \alpha) = 3.895 \left(\frac{D}{r_0}\right)^{\frac{5}{3}} \left[ \sum_{n=1}^{\infty} (n + 1)^2 I_{n,0}(0) - \sum_{n=1}^N (n + 1)^2 \times \left\{ 2 \frac{\int_0^{L_{atm}} dh C_n^2(h) I_{n,m}(\frac{\alpha h}{R})}{\int_0^{L_{atm}} dh C_n^2(h)} - I_{n,0}(0) \right\} \right]. \tag{32}$$

The integral  $I_{n,m}(x)$  of Equation (30) can be evaluated in closed form using Mellin transform techniques as proposed by Sasiela and Shelton (1993), and expressed in terms of rapidly converging series. This integral is transformed into a Mellin–Barnes integral, and is then expressed as a sum of generalized hypergeometric functions. As demonstrated by Sasiela and Shelton (1993), the properties of Mellin transforms and gamma functions are useful in problems dealing with wave propagation in turbulence. This technique is applied here to solve the integrals in Equation (30), Equation (60), and Equation (61).

The Mellin transform pair is given by

$$\begin{aligned}
 F(s) &= \int_0^\infty dK K^{s-1} f(K), \\
 f(K) &= \frac{1}{2i\pi} \int_{\sigma-\infty}^{\sigma+\infty} ds K^{-s} F(s).
 \end{aligned}
 \tag{33}$$

The general form of the integral to solve has been presented by Chassat (1989), and can be written as ( $\eta = \frac{14}{3}$ )

$$I(x) = \int_0^\infty dK K^{-\eta} J_\alpha(K) J_\gamma(K) J_\beta(xK).
 \tag{34}$$

From the properties of the Mellin transforms (Colombo, 1959; Dautray and Lions, 1987), and using  $F_n(s) = \int_0^\infty dK K^{s-1} J_n(K)$ , the integral becomes

$$I(x) = \frac{1}{(2i\pi)^2} \int_{c-\infty}^{c+\infty} \int_{c-\infty}^{c+\infty} F_\alpha(s) F_\beta(t) x^{-t} F_\gamma(-\eta - t + 1 - s) ds dt.
 \tag{35}$$

Tables of Mellin transforms (Colombo, 1959; Dautray and Lions, 1987; Sasiela and Shelton, 1993) are helpful for solving Equation (35). Moreover, the Mellin transform of functions can usually be expressed as a ratio of gamma functions. We use the following notation:

$$\Gamma \left[ \begin{matrix} x_1, x_2, \dots, x_n \\ y_1, y_2, \dots, y_m \end{matrix} \right] = \frac{\Gamma(x_1)\Gamma(x_2)\cdots\Gamma(x_n)}{\Gamma(y_1)\Gamma(y_2)\cdots\Gamma(y_m)}.
 \tag{36}$$

We have for  $J_n$  the  $n$ th-order Bessel function of the first kind:

$$F_n(s) = 2^{s-1} \Gamma \left[ \begin{matrix} \frac{s}{2} + \frac{n}{2} \\ \frac{n}{2} - \frac{s}{2} + 1 \end{matrix} \right] \quad \text{with } \text{Re}(-n) < \text{Re}(s) < \frac{3}{2}.
 \tag{37}$$

It leads to the Mellin–Barnes integral

$$\begin{aligned}
 I(x) &= \frac{1}{(2i\pi)^2} \int_{-i\infty}^{+i\infty} \int_{-i\infty}^{+i\infty} \Gamma \left[ \begin{matrix} -s - t + \frac{\alpha-\eta+1}{2}, t + \frac{\beta}{2}, s + \frac{\gamma}{2} \\ 1 + t + s + \frac{\alpha+\eta-1}{2}, 1 - t + \frac{\beta}{2}, 1 - s + \frac{\gamma}{2} \end{matrix} \right] \\
 &\quad \times 2^{-\eta} x^{-2t} ds dt.
 \end{aligned}
 \tag{38}$$

This integration can be performed using the method of pole residuals. The value of the integral, as given by Cauchy’s formula, is just  $2\pi i$  times the sum of the residuals at the enclosed poles. The result can be expressed in terms of generalized hypergeometric functions (Abramovitz and Stegun, 1965). For instance, in the interesting case  $x = \frac{\alpha h}{R} > 1$ , the integral is given by

$$I(x) = F_4 \left[ \begin{matrix} \frac{1}{2} \left( \alpha + \gamma + \beta - \frac{11}{3} \right), \frac{1}{2} \left( \alpha + \gamma - \beta - \frac{11}{3} \right), \alpha + 1, \gamma + 1 \\ \frac{1}{x^2}, \frac{1}{x^2} \end{matrix} \right]$$

$$\begin{aligned} & \times \frac{\Gamma[\frac{1}{2}(\alpha + \delta + \beta - \frac{11}{3})]}{\Gamma[\gamma + 1]} \frac{\Gamma[\frac{1}{2}(\alpha + \gamma - \beta - \frac{11}{3})]}{\Gamma[\alpha + 1]} \\ & \times \frac{(-1)^{2p+2q}}{-\pi} 2^{-\frac{11}{3}} x^{-n_i - n_j + \frac{5}{3}} \sin\left(\frac{\pi}{2}\left(\alpha + \gamma - \beta - \frac{17}{3}\right)\right), \end{aligned} \tag{39}$$

where

$$F_4(\alpha, \beta, \gamma, \gamma'; x, y) = \sum_{m=0}^{\infty} \sum_{n=0}^{\infty} \frac{(\alpha)_{m+n}(\beta)_{m+n}x^m y^n}{(\gamma)_m(\gamma')_n m! n!}$$

with the notation  $(a)_n = \frac{\Gamma(a + n)}{\Gamma(a)}$ . (40)

When the function is expressed in terms of generalized hypergeometric functions, the integral leads to the more restrictive convergence condition that can be expressed as  $\frac{\alpha h}{R} < 2$ . This condition determines the maximum field of view that can be reached using this method.

The limited convergence domain encountered in the evaluation of integrals involving the product of three Bessel functions was first remarked by Tyler (1990). Chassat (1989) proposed a method using the Bessel recurrence relation:

$$J_{\mu+2}(K) = \frac{2(\mu + 1)}{K} J_{\mu+1}(K) - J_{\mu}(K). \tag{41}$$

Two easily evaluated Mellin integrals appear:

$$\begin{aligned} I_1(x, \mu, \beta, \eta) &= \int_0^{\infty} dK K^{-\eta} J_{\mu}^2(K) J_{\beta}(Kx), \\ I_2(x, \mu, \beta, \eta) &= \int_0^{\infty} dK K^{-\eta} J_{\mu}(K) J_{\mu+1}(K) J_{\beta}(Kx). \end{aligned} \tag{42}$$

With the notation  $\mu = \inf(\alpha, \gamma)$  and  $\sigma = |\alpha - \gamma|$ , Equation (34) becomes

$$I(x) = \int_0^{\infty} dK K^{-\eta} J_{\mu} J_{\mu+\sigma}(K) J_{\beta}(xK) = I(\mu, \sigma, \eta, \beta)(x). \tag{43}$$

The Bessel recurrence relation becomes the recurrence between Mellin integrals, which can be written as

$$I(\mu, \sigma - 1, \eta, \beta) = 2(\mu + \sigma - 1)I(\mu, \sigma, \eta + 1, \beta) - I(\mu, \sigma - 2, \eta, \beta). \tag{44}$$

Now, we can use the Mellin transform tables to solve  $I(x, \mu, \beta, \eta)$ , and  $I(x, \mu, \beta, \eta)$  which can be expressed as Mellin–Barnes integrals of the following type:

$$\frac{1}{2\pi i} \int_{c-i\infty}^{c+i\infty} G(t)F(1 - t - \eta)x^{t+\eta-1} dt, \tag{45}$$

where  $G$  and  $F$  are the Mellin transforms of  $g$  and  $f$  respectively.  $g$  and  $f$  are defined as

$$\begin{cases} f(aK) = J_{\beta}(Kx) \\ g(K) = J_{\mu}^2(K) \end{cases} \quad \text{to solve } I_1(x, \mu, \beta, \eta), \tag{46}$$

$$\begin{cases} f(aK) = J_\beta(Kx) \\ g(K) = J_\mu(K)J_{\mu+1}(K) \end{cases} \quad \text{to solve } I_2(x, \mu, \beta, \eta). \tag{47}$$

We have the Mellin transforms

$$g(K) = J_\mu^2(K) \longrightarrow G(s) = \frac{1}{2\sqrt{\pi}} \Gamma \left[ \mu + 1 - \frac{s}{2}, 1 - \frac{s}{2} \right],$$

with  $\text{Re}(-2\mu) < \text{Re}(s) < 1$ , (48)

$$g(K) = J_\mu(K)J_{\mu+1}(K) \longrightarrow G(s) = \frac{1}{2\sqrt{\pi}} \Gamma \left[ \frac{s+1}{2} + \mu, 1 - \frac{s}{2} \right],$$

with  $\text{Re}(-2\mu - 1) < \text{Re}(s) < 2$ . (49)

The Mellin transform of  $f(Kx)$  is given by Equation (34). Finally, using Cauchy’s formula, we find:

If  $x \leq 2$

$$\begin{aligned} I_1(x, \mu, \beta, \eta) &= \sum_{p=0}^{\infty} \frac{1}{2\sqrt{\pi}} \frac{(-1)^p}{p!} \left(\frac{x}{2}\right)^{2p+\eta} \\ &\times \Gamma \left[ -p + \mu + \frac{1}{2}, \frac{1}{2} + p, p + \frac{\beta}{2} + 1 + \frac{\eta}{2} \right] \\ &+ \sum_{p=0}^{\infty} \frac{1}{2\sqrt{\pi}} \frac{(-1)^p}{p!} \left(\frac{x}{2}\right)^{2p+\beta} \\ &\times \Gamma \left[ \mu - p - \frac{\beta+\eta+1}{2}, \frac{1+\eta-\beta}{2} - p, p + \beta + 1 \right], \end{aligned} \tag{50}$$

$$\begin{aligned} I_2(x, \mu, \beta, \eta) &= \sum_{p=0}^{\infty} \frac{1}{2\sqrt{\pi}} \frac{(-1)^p}{p!} \left(\frac{x}{2}\right)^{2p+\eta+1} \Gamma \left[ \frac{3}{2} + \mu + p, -p - \frac{\eta+1-\beta}{2} \right] \\ &\times \Gamma \left[ \mu - p + \frac{1}{2}, \frac{1}{2} - p, p + \frac{\eta+3+\beta}{2} \right] \\ &+ \sum_{p=0}^{\infty} \frac{1}{2\sqrt{\pi}} \frac{(-1)^p}{p!} \left(\frac{x}{2}\right)^{2p+\beta} \\ &\times \Gamma \left[ \mu - p + 1 + \frac{1-\eta+\beta}{2}, \beta + p, -p + \frac{\eta+1+\beta}{2} \right] \\ &\times \Gamma \left[ \mu - p + 1 + \frac{\eta-\beta}{2}, 1 + \frac{\eta-\beta}{2} - p, p + \beta + 1 \right]. \end{aligned} \tag{51}$$

If  $x > 2$

$$\begin{aligned} I_1(x, \mu, \beta, \eta) &= \sum_{p=0}^{\infty} \frac{1}{2\sqrt{\pi}} \frac{(-1)^p}{p!} \left(\frac{x}{2}\right)^{-2p-2\mu+\eta-1} \\ &\times \Gamma \left[ \frac{1}{2} + \mu + p, p + \mu + \frac{1-\eta+\beta}{2} \right] \\ &\times \Gamma \left[ p + 2\mu + 1, p + \mu + 1, -p - \mu + \frac{\eta+1+\beta}{2} \right], \end{aligned} \tag{52}$$

$$I_2(x, \mu, \beta, \eta) = \sum_{p=0}^{\infty} \frac{1}{2\sqrt{\pi}} \frac{(-1)^p}{p!} \left(\frac{x}{2}\right)^{-2p-2\mu+\eta-2}$$

$$\times \Gamma \left[ \begin{matrix} \frac{3}{2} + \mu + p, p + \mu + 1 - \frac{x+\beta}{2} \\ p + 2\mu + 2, p + \mu + 2, -p + \mu + \frac{x+\beta}{2} \end{matrix} \right]. \tag{53}$$

**Appendix B: Derivation of the Optical Transfer Functions**

The image quality can be evaluated by comparing the restored image frequencies of the optical transfer function of an extended source. The optical transfer function after correction (OTF) can be defined as the mathematical expectation of the cross-correlation function of the complex amplitude of the compensated wavefront. Assuming that scintillation effects are negligible, this amplitude can be written as

$$\psi(\mathbf{r}) = \exp\{i\phi_c(\mathbf{r})\}, \tag{54}$$

where the wavefront after compensation  $[\phi_c(\mathbf{r})]$  is the difference between the wavefront  $[\phi(\mathbf{r})]$  coming from the observed source and the estimated wavefront reconstructed by the AO system from the measurements at angular distance  $\alpha$   $[\hat{\phi}(\mathbf{r})]$ . For the near-field approximation, the OTF can be written as

$$\text{OTF}(\mathbf{u}, \alpha) = \int d\mathbf{r} \left\langle \psi \left( \mathbf{r} + \frac{\mathbf{u}}{2} \right) \psi^* \left( \mathbf{r} - \frac{\mathbf{u}}{2} \right) \right\rangle W \left( \mathbf{r} + \frac{\mathbf{u}}{2} \right) W \left( \mathbf{r} - \frac{\mathbf{u}}{2} \right), \tag{55}$$

where  $W(\mathbf{u})$  is the normalized function defined by Equation (21). The phase is a Gaussian random function (Rodier, 1981). Equation (55) becomes

$$\begin{aligned} \text{OTF}(\mathbf{u}, \alpha) &= \int d\mathbf{r} \exp \left( -\frac{1}{2} \left\langle \left[ \phi_c \left( \mathbf{r} + \frac{\mathbf{u}}{2} \right) - \phi_c \left( \mathbf{r} - \frac{\mathbf{u}}{2} \right) \right]^2 \right\rangle \right) \\ &\times W \left( \mathbf{r} + \frac{\mathbf{u}}{2} \right) W \left( \mathbf{r} - \frac{\mathbf{u}}{2} \right). \end{aligned} \tag{56}$$

The statistics of the Zernike coefficients for an expansion of Kolmogorov turbulence phase distortion have been applied by Wang and Markey (1978) to calculate the OTF for a point source case ( $\alpha = 0$ ). We apply the OTF derived from our method to cases when the observing source is extended in order to evaluate the degradation in the field of view of the image due to anisoplanatism after AO compensation.

Using Equations (19) and (24) for the wavefront expansions, the argument of the exponential of Equation (56) can be expressed as

$$\begin{aligned} E(\mathbf{r}, \mathbf{u}) &= -\frac{1}{2} \left\langle \left[ \phi \left( \mathbf{r} + \frac{\mathbf{u}}{2} \right) - \phi \left( \mathbf{r} - \frac{\mathbf{u}}{2} \right) \right]^2 \right\rangle - \frac{1}{2} \left\langle \left[ \hat{\phi} \left( \mathbf{r} + \frac{\mathbf{u}}{2} \right) - \hat{\phi} \left( \mathbf{r} - \frac{\mathbf{u}}{2} \right) \right]^2 \right\rangle \\ &+ \left\langle \left[ \hat{\phi} \left( \mathbf{r} + \frac{\mathbf{u}}{2} \right) - \hat{\phi} \left( \mathbf{r} - \frac{\mathbf{u}}{2} \right) \right] \left[ \phi \left( \mathbf{r} + \frac{\mathbf{u}}{2} \right) - \phi \left( \mathbf{r} - \frac{\mathbf{u}}{2} \right) \right] \right\rangle. \end{aligned} \tag{57}$$

We recognize the first term as the wave structure function. For a Kolmogorov-type turbulence, the wave structure function can be expressed as

$$\left\langle \left[ \phi \left( \mathbf{r} + \frac{\mathbf{u}}{2} \right) - \phi \left( \mathbf{r} - \frac{\mathbf{u}}{2} \right) \right]^2 \right\rangle = D(\mathbf{u}) = 6.88 \left( \frac{u}{r_0} \right)^{5/3}. \tag{58}$$

We introduce the notation

$$H_{i,j}(\mathbf{r}, \mathbf{u}) = \left[ Z_i\left(\mathbf{r} + \frac{\mathbf{u}}{2}\right) - Z_i\left(\mathbf{r} - \frac{\mathbf{u}}{2}\right) \right] \left[ Z_j\left(\mathbf{r} + \frac{\mathbf{u}}{2}\right) - Z_j\left(\mathbf{r} - \frac{\mathbf{u}}{2}\right) \right]. \tag{59}$$

The cross-correlations of the Zernike coefficients [ $\langle a_i a_j \rangle(\alpha)$ ] are calculated when the reference source target is at angular distance  $\alpha$  from the observed source for  $J$  corrected modes by the AO system. The turbulence profiles  $C_n^2$  used in the calculation of the angular cross-correlation are presented in Figure 3:

$$\left\langle \left[ \hat{\phi}\left(\mathbf{r} + \frac{\mathbf{u}}{2}\right) - \hat{\phi}\left(\mathbf{r} - \frac{\mathbf{u}}{2}\right) \right]^2 \right\rangle = \sum_{i=2}^J \sum_{j=2}^J \langle a_i a_j \rangle H_{i,j}(\mathbf{r}, \mathbf{u}), \tag{60}$$

$$\left\langle \left[ \phi\left(\mathbf{r} + \frac{\mathbf{u}}{2}\right) - \phi\left(\mathbf{r} - \frac{\mathbf{u}}{2}\right) \right] \left[ \hat{\phi}\left(\mathbf{r} + \frac{\mathbf{u}}{2}\right) - \hat{\phi}\left(\mathbf{r} - \frac{\mathbf{u}}{2}\right) \right] \right\rangle = \sum_{i=2}^{\infty} \sum_{j=2}^J \langle a_i a_j \rangle(\alpha) H_{i,j}(\mathbf{r}, \mathbf{u}). \tag{61}$$

The OTF in the field of view is obtained by evaluating the following numerical expression as indicated by Wang and Markey (1978):

$$\text{OTF}(\mathbf{u}, \alpha) = \frac{4}{\pi} \int_0^{\pi/2} d\theta \int_0^{r_{\max}} dr r \exp[E(\mathbf{r}, \mathbf{u})], \tag{62}$$

with

$$\begin{aligned} E(\mathbf{r}, \mathbf{u}) \approx & -\frac{1}{2} D(\mathbf{u}) + \sum_{i=2}^J \sum_{j=2}^J \left[ \langle a_i a_j \rangle(\alpha) - \frac{1}{2} \langle a_i a_j \rangle \right] H_{i,j}(\mathbf{r}, \mathbf{u}) \\ & + \sum_{i=J+1}^{J_{\text{limit}}} \sum_{j=2}^J \langle a_i a_j \rangle(\alpha) H_{i,j}(\mathbf{r}, \mathbf{u}) \end{aligned} \tag{63}$$

and

$$r_{\max} = -\frac{u}{2} \cos(\theta - \varphi) + \sqrt{1 - \left[ \frac{u}{2} \sin(\theta - \varphi) \right]^2}, \tag{64}$$

where  $\varphi$  is the argument of  $\mathbf{u}$ .

To characterize the quality of the image, we use the Fried resolution criteria (Fried, 1966):

$$\mathcal{R} = \int \text{OTF}(\mathbf{f}) d\mathbf{f}. \tag{65}$$

The quantity  $\mathcal{R}$  is proportional to the Strehl ratio [ $Sr$ ] defined by

$$Sr = \frac{\int \text{OTF}(\mathbf{f}) d\mathbf{f}}{\int T(\mathbf{f}) d\mathbf{f}}, \tag{66}$$

where  $T$  is the transfer function of the telescope ( $T = 1$  without atmosphere).

The resolution angle associated with  $\mathcal{R}$  is then (Roddier, 1981)

$$\omega = \left( \frac{4}{\pi \mathcal{R}} \right)^{1/2} = \frac{4}{\pi} \frac{\lambda}{D} \frac{1}{\sqrt{Sr}}. \tag{67}$$

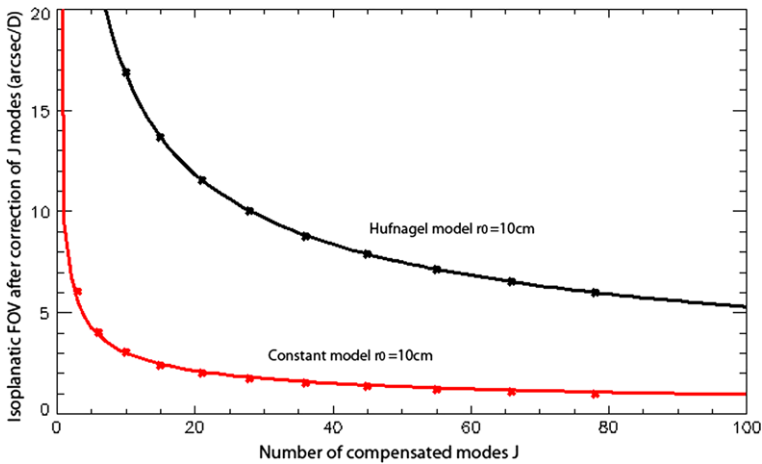


**Figure 12** Isoplanatic FOV after AO compensation of  $J$  modes versus  $J$  from 1 up to 100 modes. Curves are computed with the Hufnagel [ $C_n^2$ ] turbulence profile ( $r_0 = 10$  cm at  $\lambda = 0.5 \mu\text{m}$ ) (upper curve in black), and a constant profile (one turbulent layer) with an equivalent Fried parameter (bottom curve in red). Superimposed stars correspond to the exact derivations. Lines are derived from the asymptotic behavior.

At the diffraction limit, one obtains

$$\omega_d = \frac{4}{\pi} \frac{\lambda}{D} = 1.27 \frac{\lambda}{D}. \tag{68}$$

**Appendix C: Effect of the Turbulence Profile on the Derivations**

In Figure 12 we show the small effect of the distribution of the turbulent layers when dealing with high-order modes of a classical AO system. The modal behavior of the AO (*i.e.*, for a large number of corrected modes) depends roughly on the mean turbulence profile summation. The choice for the atmospheric turbulence profile becomes marginal, with regard to the very large ratio between the required field of view (FOV) for the science case that we study and our calculated isoplanetic domain. Figure 12 shows the derivation obtained for a constant-turbulence model made of a single layer with an equivalent Fried parameter. The isoplanetic domain is half the value obtained with the Hufnagel profile for a large number of modes ( $> 1000$ ), and remains very small (around one arcsecond). The isoplanetic angle and the Fried parameter are critical parameters for the design of classical AO systems. The  $C_n^2$  profile structure is required for the tomographic reconstruction developed for MCAO, and will be the parameter used to compare sites for future wide-field AO systems (Fusco and Costille, 2010). Note that the best solar observations are obtained early in the morning with night-like conditions, as indicated by the measurements of (Barletti *et al.*, 1973) during the Joint Organization for Solar Observations (JOSO) campaign, that are instructive in showing the continuity from night to day. The turbulence is fully developed as the Sun rises to the zenith. The ground-layer turbulence adds to the night model (increasing with the heat of the Sun).

The Hufnagel profile is a widely used turbulence model; it is accessible to any researcher who wants to validate the theory. Statistical studies of the input parameters of the turbulence

above the Canary Island observatories using meteorological databases have been compared to the modeling (Chueca *et al.*, 2004). At the Haleakala site, a median value of  $r_0$  of 9.7 cm, the result of 92 307 measurements for 651 days from January 2002 to August 2004, has been derived for daytime measurements (Bradley *et al.*, 2006). The Hufnagel model  $C_n^2(h)$  is given by

$$2.72 \times 10^{-16} \left[ 3 \left( \frac{V}{27} \right)^2 \left( \frac{h}{10} \right)^{10} \exp(-h) \right] + 10^{-16} \left( \frac{h}{1.5} \right)^{-\frac{2}{3}}, \quad (69)$$

with an altitude  $h$  expressed in kilometers and with wind velocity  $V$  in  $\text{m s}^{-1}$ . The profile is integrated from 10 m to 20 000 m to obtain a Fried's parameter  $r_0 = 10$  cm at  $\lambda = 0.5 \mu\text{m}$ .

## References

- Abramovitz, M., Stegun, I.A.: 1965, *Handbook of Mathematical Functions*, Dover, New York.
- Archontis, V., Hood, A.W.: 2009, *Astron. Astrophys.* **508**, 1469.
- Aubailly, M., Roggeman, M.C., Schultz, T.J.: 2007, *Appl. Opt.* **46**, 6055.
- Aulanier, G., Schmieder, B.: 2002, *Astron. Astrophys.* **386**, 1106.
- Aulanier, G., Torok, T., Démoulin, P., DeLuca, E.E.: 2010, *Astrophys. J.* **708**, 314.
- Barletti, R., Ceppatelli, G., Moroder, E., Paterno, L., Righini, A.: 1973, J.O.S.O. Annual Report, Bratislava, 74.
- Beck, C., Rezaei, R.: 2009, *Astron. Astrophys.* **502**, 969.
- Berkefeld, T.: 2006, *SPIE* **6272**, 4.
- Bradley, E.E., Roberts, L.C., Bradford, L.W., Skinner, M.A., Nahestedt, D.A., Waterson, M.F., Kuhn, J.R.: 2006, *Publ. Astron. Soc. Pac.* **118**, 172.
- Bommier, V., Landi Degl'Innocenti, E., Landolfi, M., Molodij, G.: 2007, *Astron. Astrophys.* **464**, 323.
- Cao, W., Gorceix, N., Coulter, R., Ahn, K., Rimmele, T.R., Goode, P.R.: 2010, *Astron. Nachr.* **331**, 636.
- Canou, A., Amari, T., Bommier, V., Schmieder, B., Aulanier, G., Li, H.: 2009, *Astrophys. J.* **693**, 27.
- Canou, A., Amari, T.: 2010, *Astrophys. J.* **715**, 1566.
- Chassat, F.: 1989, *J. Opt. (Paris)* **20**, 13.
- Cheung, M.C., Rempel, M., Title, A.M., Schussler, M.: 2010, *Astrophys. J.* **720**, 233.
- Chueca, S., Garcia-Lorenzo, B., Mendizabal, E.G., Varela, T., Fuensalida, J.J., Munoz-Tunon, C.: 2004, *SPIE* **5237**, 159.
- Colombo, S.: 1959, *Les transformations de Mellin et de Hankel*, C.N.R.S, Paris.
- Conan, J.M., Madec, P.Y.: 1994, *J. Opt. Soc. Am. A* **12**, 1559.
- Costille, A., Conan, J.M., Kulcsar, C., Raynaud, H.F., Fusco, T.: 2010, *J. Opt. Soc. Am. A* **27**, 3.
- Dautray, R., Lions, J.L.: 1987, *Transformations de Mellin, Analyse Mathématique et Calcul Numérique*, Paris, Masson, 3.
- Fried, D.L.: 1966, *J. Opt. Soc. Am. A* **56**, 1372.
- Fried, D.L.: 1962, *J. Opt. Soc. Am. A* **72**, 52.
- Fusco, T., Costille, A.: 2010, *SPIE* **7736**, 159.
- Gendron, E., Léna, P.: 1994, *Astron. Astrophys.* **291**, 337.
- Gendron, E., Vidal, F., Brangier, M., Morris, T., Hubert, Z., Basden, A., Rousset, G., Myers, R., Chemla, F., Longmore, A., Butterley, T., Dipper, N., Dunlop, C., Geng, D., Grataudour, D., Henry, D., Laporte, P., Looker, N., Perret, D., Sevin, A., Talbot, G., Younger, E.: 2011, *Astron. Astrophys. Lett.* **529**, L2.
- Hufnagel, R.E.: 1974, In: *OSA Technical Digest Series, Optical Propagation Through Turbulence*, OAS, Washington, WA1-1.
- Lagrange, A.-M., Chauvin, G., Fusco, T., Gendron, E., Rouan, D., Hartung, M., Lacombe, F., Mouillet, D., Rousset, G., Drossart, P., Lenzen, R., Moutou, C., Brandner, W., Hubin, N., Clenet, Y., Stolte, A., Schoedel, R., Zins, G., Spyromilio, J.: 2003, *SPIE* **4841**, 860.
- Kuckein, C., Centeno, R., Martinez Pillet, V.: 2010, *Mem. Soc. Astron. Ital.* **81**, 668.
- Langlois, M., Moretto, G., Richards, K., Hegwer, S., Rimmele, T.R.: 2004, *SPIE* **5490**, 59.
- Léna, P.: 1994, *SPIE* **2201**, 1099.
- Lionello, R., Mikic, Z., Linker, J.A., Amari, T.: 2002, *Astrophys. J.* **581**, 718.
- Low, B.C., Wolfson, B.: 1988, *Astrophys. J.* **324**, 574.
- Masson, S., Pariat, E., Aulanier, G., Schrijver, C.J.: 2009, *Astrophys. J.* **700**, 559.

- Metcalf, T.R., De Rosa, M.L., Schrijver, C.J., Barnes, G., Van Ballegooijen, A.A., Wiegmann, T., Wheatland, M.S., Valori, G., McTiernan, J.M.: 2008, *Solar Phys.* **247**, 269.
- Molodij, G., Rayrole, J., Madec, P.Y., Colson, F.: 1998, *Astron. Astrophys. Suppl. Ser.* **118**, 169.
- Molodij, G., Rousset, G.: 1997, *J. Opt. Soc. Am. A* **14**, 1949.
- Molodij, G., Rayrole, J.: 1998, *Astron. Astrophys. Suppl. Ser.* **128**, 229.
- Molodij, G.: 2011, *J. Opt. Soc. Am. A* **28**, 8, 1732.
- Moreno-Insertis, F., Galsgaard, K., Ugarte-Urra, I.: 2009, In: Lites, B., Cheung, M., Magara, T., Mariska, J., Reeves, K. (eds.) *The Second Hinode Science Meeting: Beyond Discovery-Toward Understanding CS-415*, Astron. Soc. Pac., San Francisco, 51.
- Noll, R.J.: 1976, *J. Opt. Soc. Am. A* **66**, 207.
- Pariat, E., Aulancier, G., Schmieder, B., Georgoulis, M.K., Rust, D.M., Bernasconi, P.N.: 2004, *Astrophys. J.* **614**, 1099.
- Roddir, F.: 1981, In: Wolf, E. (ed.) *The Effect of Atmospheric Turbulence in Optical Astronomy, Progress in Optics*, **19**, North-Holland, Amsterdam, 281.
- Rousset, G.: 1993, In: Alloin, D., Mariotti, J.M. (eds.) *Adaptive Optics for Astronomy. NATO ASI Series*, Kluwer Academic, Dordrecht, 115.
- Rimmele, T.: 2006, *SPIE* **6272**, 5.
- Rimmele, T., Hegwer, S., Marino, J., Richards, K., Schmidt, D., Waldmann, T., Woeger, F.: 2010, In: Clenet, F., Rousset, G. (eds.) *1st AO4ELT Conference Adaptive Optics for Extremely Large Telescope*, EDP Sciences, Paris, 125.
- Sanakarasubramanian, K., Rimmele, T.: 2008, *J. Astrophys. Astron.* **29**, 329.
- Sasiela, R.J.: 1988, A unified approach to electromagnetic wave propagation in turbulence and evaluation of multiparameter integrals. Tech Rep 807, M.I.T Lincoln Laboratory, Lexington, Mass.
- Sasiela, R.J., Shelton, J.D.: 1993, *J. Opt. Soc. Am. A* **10**, 647.
- Schrijver, C.J., De Rosa, M.L., Metcalf, T., Barnes, G., Lites, B., Tarbell, T., McTiernan, J., Valori, G., Wiegmann, T., Wheatland, M.S., Amari, T., Aulancier, G., Démoulin, P., Fuhrmann, M., Kusano, K., Régnier, S., Thalmann, J.K.: 2008, *Astrophys. J.* **675**, 1637.
- Tyler, G.A.: 1990, *J. Opt. Soc. Am. A* **7**, 1218.
- Valley, G.C., Wandzura, S.M.: 1979, *J. Opt. Soc. Am. A* **69**, 712.
- Van Ballegooijen, A.A., Martens, P.C.H.: 1989, *Astrophys. J.* **343**, 971.
- Wang, J.Y., Markey, J.K.: 1978, *J. Opt. Soc. Am. A* **68**, 79.